Supplementary Information

Ligand entry pathways control the chemical space recognized by GPR183

Viktoria Madeline Skovgaard Kjær[+,a], Tomasz Maciej Stępniewski[+,b,c,d], Brian Medel-Lacruz [b], Lisa Reinmuth[a], Marija Ciba[e], Elisabeth Rexen Ulven[e], Massimiliano Bonomi[f], Jana Selent*[,b] and Mette Marie Rosenkilde*[a]

[a] V. M. S. Kjær, L. Reinmuth, Prof. M. M. Rosenkilde
Department of Biomedical Sciences, Faculty of Health and Medical Sciences
University of Copenhagen
Blegdamsvej 3B, 2200 København N, Danmark

[b] T. M. Stępniewski, B. Medel-Lacruz, J. Selent
Research Programme on Biomedical Informatics (GRIB), Hospital del Mar Medical Research Institute (IMIM)
& Pompeu Fabra University (UPF)
Dr. Aiguader 88, E-8003 Barcelona, España

[c] T. M. Stępniewski
InterAx Biotech AG
PARK innovAARE, 5234 Villigen, Switzerland

[d] T. M. Stępniewski
Biological and Chemical Research Centre, Faculty of Chemistry
University of Warsaw
02-089, Warsaw, Poland

[e]. M. Ciba, E. R. Ulven
Department of Drug Design and Pharmacology
University of Copenhagen
Jagtvej 160, 2100 København Ø, Danmark

[f] M. Bonomi
Institut Pasteur, Université Paris Cité, CNRS UMR3528,
Structural Bioinformatics Unit,
75015 Paris, France

[+] These authors contributed equally to this work
[*] Corresponding authors Jana Selent (jana.selent@upf.edu) and Mette Rosenkilde (Rosenkilde@sund.ku.dk)

Table of contents:

1. Methods

We used metadynamics simulations to investigate the binding and unbinding behavior of 7α,25-OHC from the orthosteric binding pocket towards the membrane. The simulations were carried out by using a combination of multiple walkers, well-tempered metadynamics and funnel metadynamics using GROMACS 2022.5 [PMID: 16211538] and the open-source, community-developed PLUMED library[1],version 2.8[2].

The funnel was employed as a guiding potential to steer the ligand along the desired pathways in both the lower leaflet and upper leaflet regions during the simulations. We followed the detailed protocol described in the funnel metadynamics paper[3].

The collective variable (CV) used in this study describes the distance between the ligand and the orthosteric binding pocket. In detail, we used the distance between the center of mass of the ligand's heavy atoms and the center of the Cα atoms of the residues located at 6 Å around the crystallized pose of 7α,25-OHC in the orthosteric binding pocket (PDB: 7TUZ). This includes the following residues Tyr112, Ile113, Tyr116, Val159, Gln162, Thr163, Leu166, Met182, Glu183, Tyr184, Leu197, Ala200, Cys201, Ile203, Gly204, Leu290, His291 and Val294. The funnel restraint was shaped to include the entire binding pocket as well as the proposed lateral channel between TM 3 to 5 either oriented to the upper or lower leaflet.

To obtain representative frames of the ligand unbinding process in both pathways, a preliminary metadynamics simulation was performed for each case. Eight representative frames of the unbinding process were extracted from these simulations and used as the starting points for subsequent multiple walker (MW) simulations in the final metadynamics simulations.

The well-tempered metadynamics approach was employed with a Gaussian width (sigma) of 0.5 Å and a Gaussian height of 2 kJ/mol. A bias factor of 30 and a rate of Gaussian deposition of 500 steps were applied during the simulations. To enhance sampling, eight MW simulations were carried out, each running for 125 ns, resulting in a total simulation time of 1 microsecond. Each MW simulation started from one of the representative structures obtained from the ligand unbinding path. Furthermore, an upper wall restraint was imposed on the simulation, constraining the root mean square deviation (RMSD) to the backbone atoms, excluding transmembrane segments 3, 4, and 5, within a 2 Å range. This restraint aimed to maintain the overall structural integrity while allowing flexibility in the relevant regions. The free energy surfaces were calculated using plumed sum_hills function and corrected the funnel restrains by following the protocol described in the funnel metadynamics paper[3].

2. Supplementary Figures

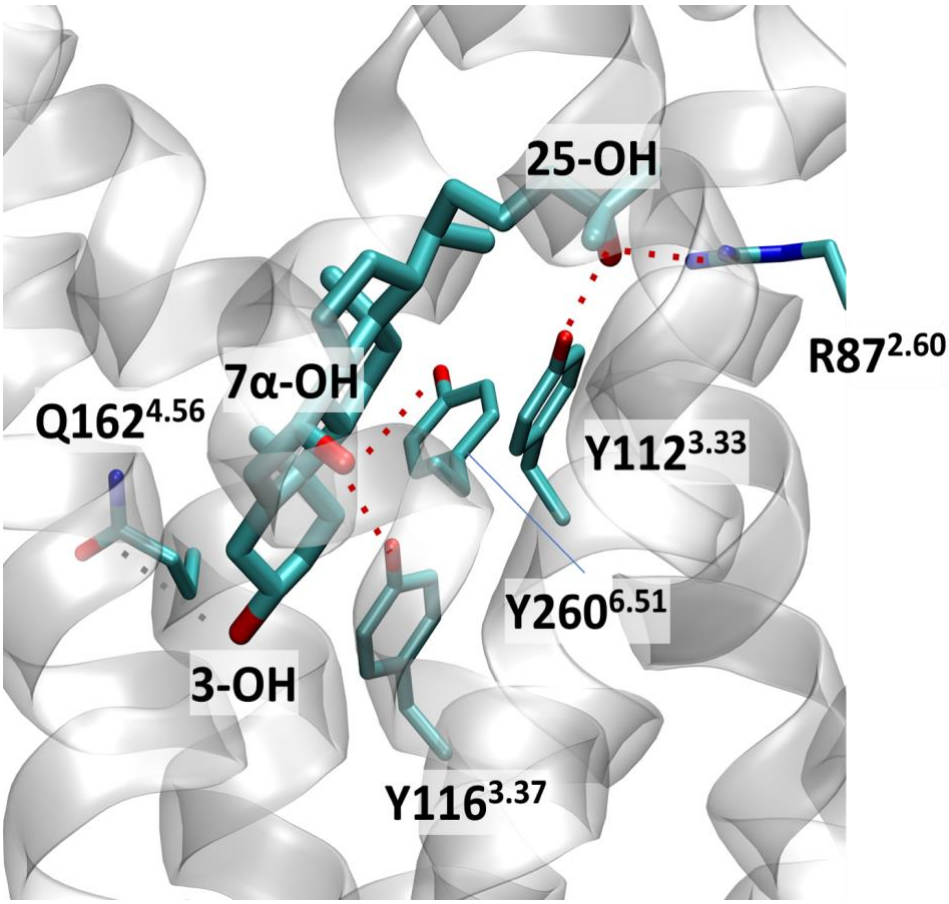

Figure S1. Binding mode of 7α,25-OHC as observed in the crystal structure (PDB ID 7TUZ). Polar interactions are highlighted using red dotted lines.

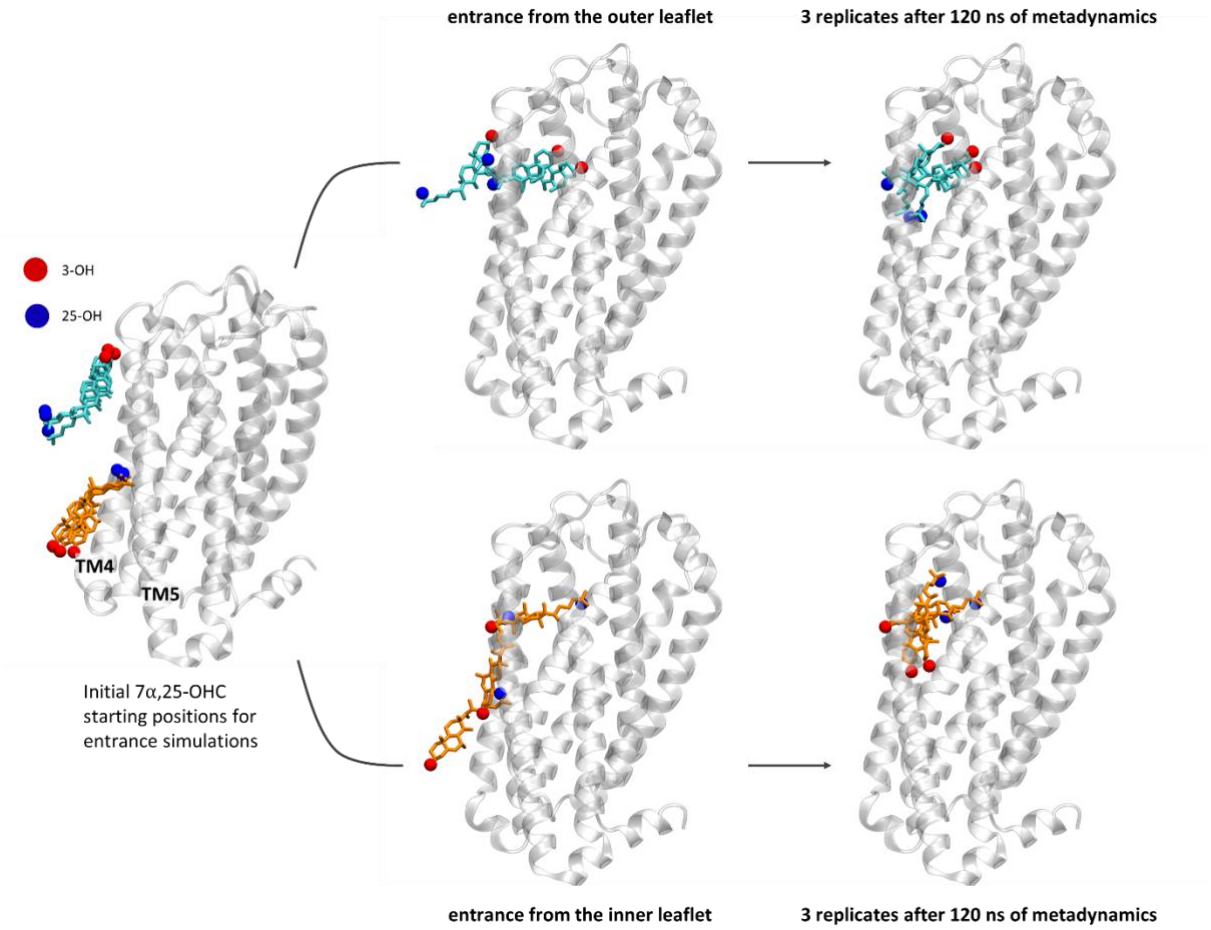

Figure S2. Probing the entrance of 7α,25-OHC into GPR183 from the extracellular and intracellular membrane leaflet. Initial starting configurations for entrance simulations using metadynamics are shown on the left panel. From the extracellular leaflet, 7α,25-OHC typically enters with the 3-OH group ahead (top). In contrast from the intracellular leaflet (bottom), 7α,25-OHC tends to enter with the 25-OH in the aliphatic tail first as observed in three replicates, respectively.

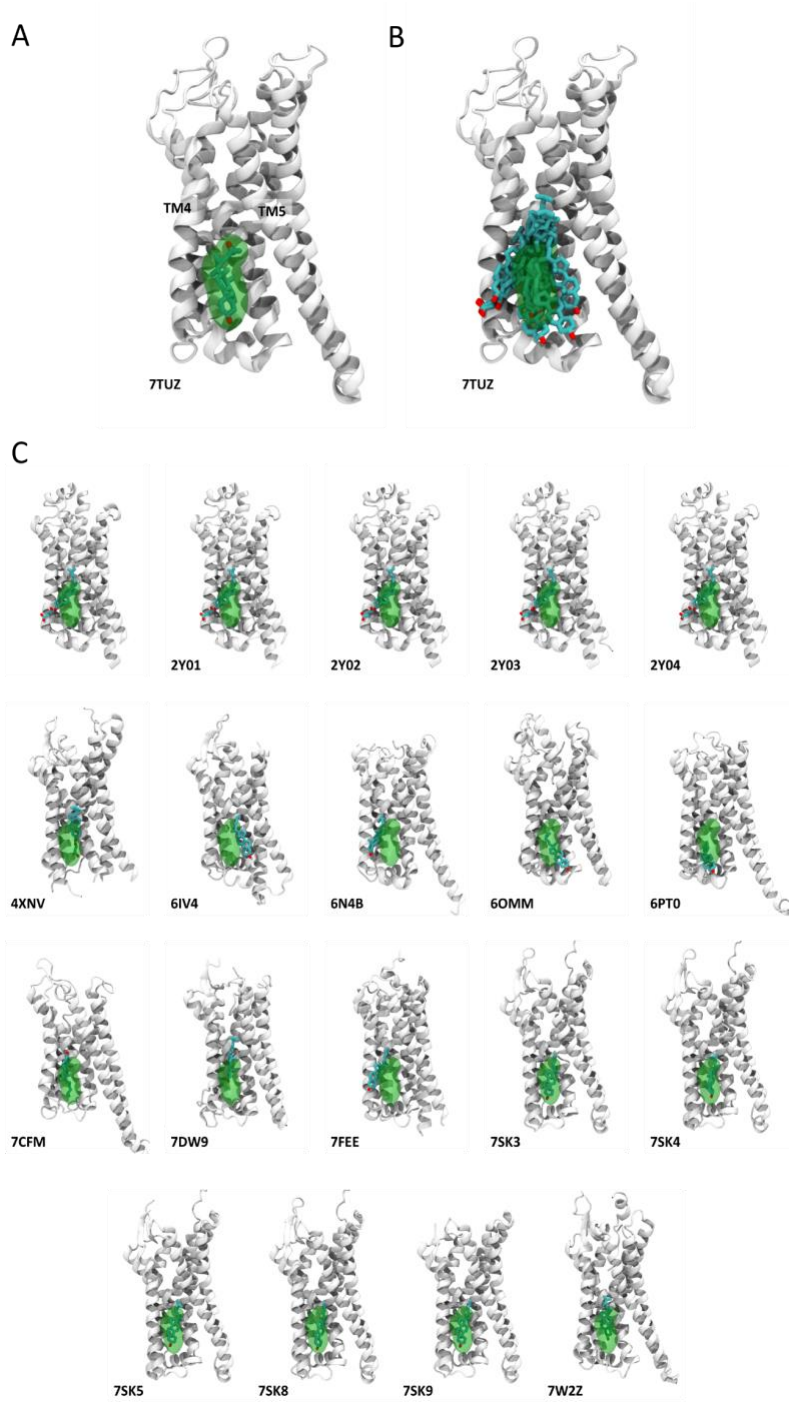

Figure S3. Structures of GPCRs with sterol molecules bound in the intracellular crevice between TM4 and TM5. A) Structure of GPR183, with a 7α,25-OHC placed in the initial anchoring mode identified through MD simulations. The molecule is depicted using cyan licorice and a green transparent surface. B) Sterol-like molecules bound to GPCRs, occupying the intracellular crevice between TM4 and TM5. Identified GPCR structures bound to a sterol-like molecule were aligned to GPR183 using backbone atoms. Sterol molecules located within the intracellular crevice between TM4 and TM5 are depicted in cyan licorice. The initial anchoring point of 7α,25-OHC within GPR183 is shown as green transparent surface, to facilitate comparison. C) Individual representation of each crystal structure with a sterol molecule bound in the intracellular crevice between TM4 and TM5. For comparison, we depicted the initial anchoring mode of 7α,25-OHC using green transparent surface.

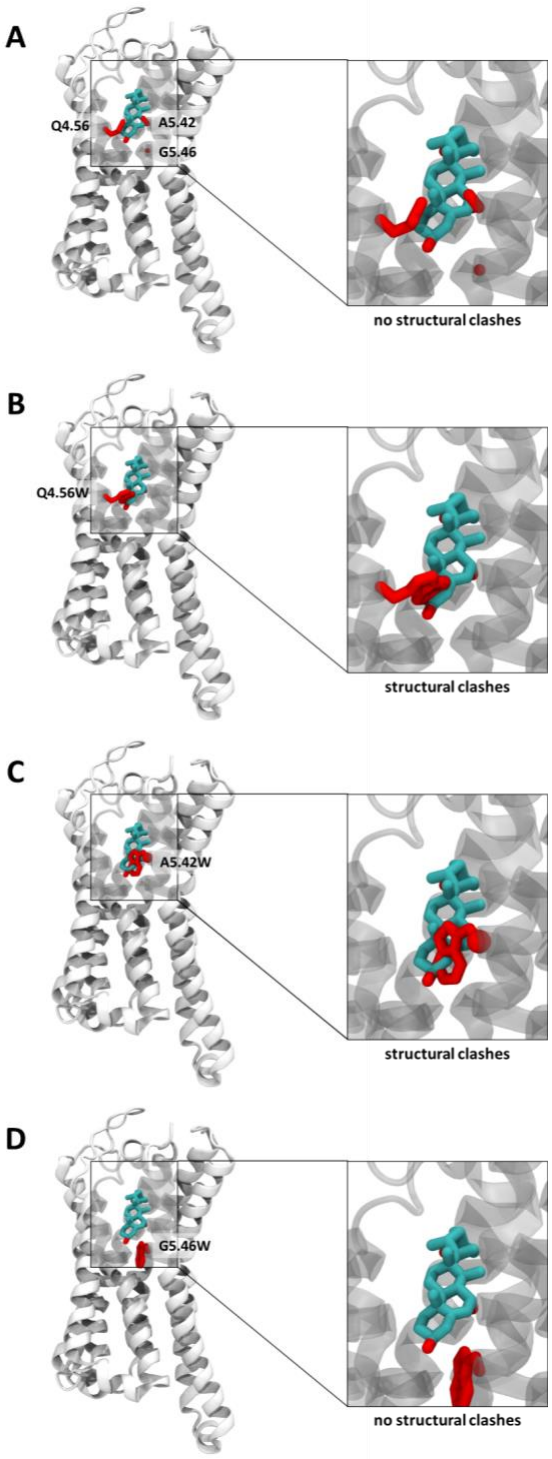

Figure S4. Analysis of mutants designed to obstruct lateral 7α,25-OHC entry into GPR183. A). Depiction of the three residues chosen to mutate into Q4.56W, A5.42W and G5.46W in order to aggravate 7α,25-OHC entry into GPR183. B-D). In each of these panels, we removed the ligand, mutated the studied residues, and then carried out a short minimization within the MOE software package (Chemical Computing Group 2022), then we introduced the crystallized pose of the ligand to monitor for clashes.

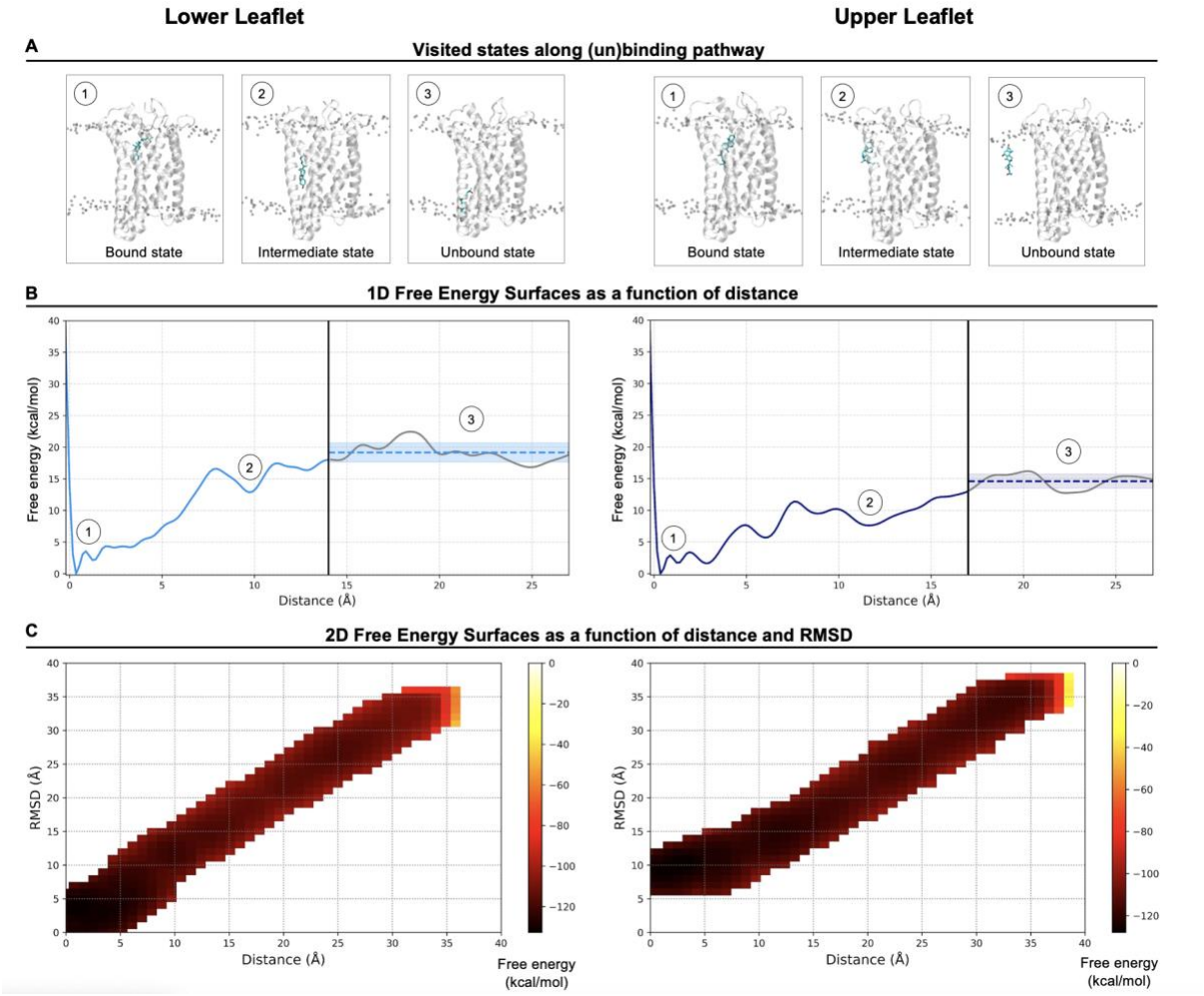

Figure S5. Estimated free energy profiles of 7α,25-OHC binding to GPR183 entry through the lower or upper membrane leaflet. These free energy profiles were obtained using well-tempered funnel metadynamics (see methods) (A) Representative frames depicting different states along the unbinding pathway of 7α,25-OHC ligand. State 1 represents the bound state in the orthosteric pocket, state 2 reflects a representative pose of an intermediate state just before the ligand enters the receptor, and state 3 is a random pose of the unbound ligand. (B) Free energy surfaces illustrate the (un)binding process of 7α,25-OHC ligand through the lower and upper leaflets of the membrane. The free energy surface is a function of the distance of the ligand from the binding pocket (for more detailed information see the method part). The numeric labels shown on the surface correspond to the snapshots shown in panel A. The free energy surfaces were calculated using the sum_hills feature of the PLUMED library (see also methods). The free energy of the unbound region should be ideally a flat region. However, due to the membrane environment, the convergence requires simulation times that are out of the scope of this study. To estimate the free energy difference between bound and unbound states, we used the mean energy value of the unbound regions (depicted in the plot with standard deviation distribution). Based on this assumption, we also estimated the difference between the binding free energy between the upper and lower leaflet systems with a value of approximately 3.9 kcal/mol. This value has been corrected considering the contribution of the bias exerted by the funnel restraint. (C) Free energies as function of the RMSD (Root Mean Square Deviation) of the ligand relative to the crystal structure 7TUZ and the distance of the ligand from the binding pocket. The free energies were computed by reweighting the metadynamics simulation using the REWEIGHT_BIAS and HISTOGRAM functions of the PLUMED library. These free energies demonstrate that RMSD values close to 0 are observed for the lower leaflet (un)binding, whereas such clusters are not evident for the upper leaflet (un)binding.

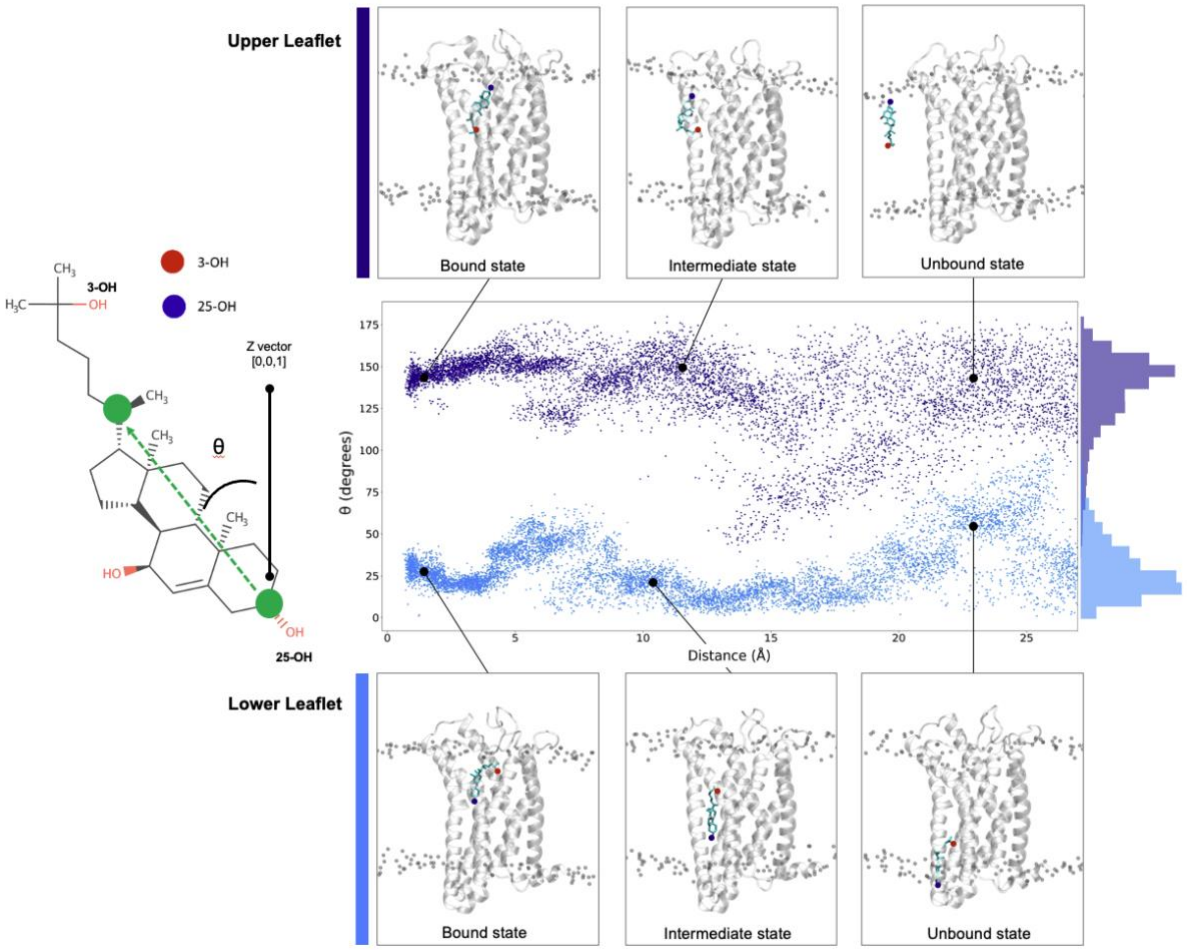

Figure S6. Ligand orientation during ligand (un)binding from the upper (dark blue) and lower (light blue) leaflet. The angle (formed between the ligand vector highlighted atoms in the sterol bulk moiety and the Z normal vector) was computed along the binding pathway to monitor ligand orientation. The final angle distribution is plotted on the right side. Structural depictions of the bound and unbound ligand at the receptor surface and in the bulk are shown. For better visualization, the 3-OH group on the aliphatic chain is highlighted by a red sphere and the 25-OH of the sterol fragment is shown as a blue sphere. Despite observing ligand flexibility and small rotational movements, the ligand did not perform a full rotation along the z-axis (i.e. a full orientational flip) neither when starting from the extracellular nor intracellular leaflet. Consequently, the ligand adopts two different final orientations in the orthosteric pocket when starting from the upper or lower leaflet.

3. Supplementary Table

Table S1: Overview of previously published signaling and binding data regarding ligand contact points within GPR183.

Receptor variant	*Homologous competition binding*	*G protein signaling (see reference for method)*		*Reference*	*Clusters****
	-logIC_{50} ± SEM	*-logEC_{50} ± SEM*			
WT	7.6 ± 0.2	9.0 ± 0.1			
R87A	N/A	5.3 ± 0.2			-
R87K	8.1 ± 0.5	7.4 ± 0.3			-
D77R R87A	7.0 ± 0.2	N/D*			-
Y112A	8.1 ± 0.5	5.8 ± 0.1		Benned-Jensen et al. 2012	1, 2, 3
Y112F	7.7 ± 0.2	8.5 ± 0.2			1, 2, 3
Y116A	N/A	<5			1, 2, 3
Y116F	N/A	<5			1, 2, 3
Y260A	N/A	<5			1, 2, 3
Y260F	N/A	5.6 ± 0.2			1, 2, 3
Q287A	N/D	N/D*			1
	% of WT ± SEM	*EC_{50} (nM ± SEM)*	*E_{max} (% of WT ± SEM)*		
WT	100	0.11 ± 0.03	100		
R87A	N/A	49.04 ± 7.72	49.97 ± 1.01		-
R87K	78.02 ± 9.35	3.99 ± 0.36	78.21 ± 1.43	Zhang et al. 2012	-
R87W	17.59 ± 8.72	64.01 ± 4.01	76.17 ± 0.86		-
Y112A	9.39 ± 4.04	11.42 ± 2.49	96.01 ± 3.22		1, 2, 3
Y116A	N/A	9.13 ± 0.92	51.71 ± 4.99		1, 2, 3
Y260A	N/A	140.50 ± 6.87	125.90 ± 2.15		1, 2, 3
		Normalized GTP turnover (% of WT)**			
WT	N/D	100			-
R87A	N/D	60			-
Y112A	N/D	63		Chen et al. 2022	1, 2, 3
Y116A	N/D	65			1, 2, 3
Y260A	N/D	68			1, 2, 3

N/A is written in cases where the value could not be reliably determined due to lack of binding. N/D signifies experiments that were not carried out.
*The signaling profiles of these variants were described by β-arrestin assays.
**These data were manually estimated from the graphs in the reference.

***clusters are indicated where the mutated residue is interacting with 7α,25-OHC

4. References

1. M. Bonomi *et al*. PLUMED consortium. Promoting transparency and reproducibility in enhanced molecular simulations. *Nat Methods*., 2019; **16**, 670-673.

2. Gareth AJ. Plumed 2: New feathers for an old bird. *Comp. Phys. Comm*. 2014,**185**, 604-13.

3. Raniolo S, Limongelli V. Ligand binding free-energy calculations with funnel metadynamics. *Nat Protoc*., 2020, **15**, 2837-2866.